Solar Energy Materials & Solar Cells 235 (2022) 111451

Contents lists available at ScienceDirect

Solar Energy Materials and Solar Cells

journal homepage: www.elsevier.com/locate/solmat

Copper iodide nanoparticles as a hole transport layer to CdTe photovoltaics: 5.5 % efficient back-illuminated bifacial CdTe solar cells

Dipendra Pokhrel, Ebin Bastola, Kamala Khanal Subedi, Suman Rijal, Manoj K. Jamarkattel, Rasha A. Awni, Adam B. Phillips, Yanfa Yan, Michael J. Heben, Randy J. Ellingson *

Wright Center for Photovoltaics Innovation and Commercialization, Department of Physics and Astronomy, The University of Toledo, OH, 43606, USA

ARTICLE INFO

Keywords:
Cadmium telluride
Back contact
Hole transport layer
Bifacial
Copper iodide (CuI)

ABSTRACT

We report the role of copper iodide (CuI) nanoparticles (NPs) as a hole transport layer (HTL) in cadmium sulfide/cadmium telluride (CdS/CdTe) photovoltaics. These CuI NPs were prepared using solution processing at room temperature and used to fabricate monofacial and bifacial CdTe solar cells with different back contacts. Using CuI/Au as the back contact, the device efficiency reached to 14.8% with outstanding fill factor (FF) of 79.2%. Replacing the gold (Au) electrode with sputtered transparent indium tin oxide (ITO), a CuI/ITO back contact yielded photoconversion efficiencies (PCEs) of 11.6% and 5.5% under front and back illumination respectively. Bifacial devices (CdTe/ITO) without the CuI NP HTL have an efficiency of 7.0% and 1.0% for front and back illumination, respectively. For CuI/ITO, a current collection of 12.0 $mAcm^{-2}$ was observed upon back illumination which significantly improved over an ITO-only back contact (5.0 $mAcm^{-2}$). The PCE obtained from back illumination was enhanced when using CuI NPs as the HTL due to the reduced back barrier height, and improved back interface as determined by temperature dependent current vs. voltage characteristics and impedance spectroscopy analysis. The improvement in device performance of the bifacial configuration is a significant step forward toward realizing thin film photovoltaic modules which harvest energy incident on the rear of the module.

1. Introduction

Cadmium telluride (CdTe), an attractive absorber layer material for solar cells with direct band gap of 1.45 eV and visible light absorption coefficient $>10^5$ cm^{-1}, is a well-known technology for fabrication of highly efficient solar cells [1]. The front and back interfaces must perform well to enable fabrication of highly efficient monofacial and bifacial devices. However, fabrication of an ohmic back contact for extraction of holes at the back interface of conventional p-type CdTe devices is challenging due to CdTe's high electron affinity and lack of suitable electrode material with deep work function [2]. Implementing a back buffer layer between CdTe and a metal electrode commonly improves performance over any direct-on-CdTe electrode [3]. Back interface recombination losses can be reduced through optimal band alignment, to repel electrons, and/or with interface passivation of defects which act as recombination sites. In addition, the output power of a photovoltaic (PV) device can be enhanced by fabricating bifacial architectures which also utilize the light incident on the back of the device. However, bifacial solar cells require that all of the materials used as a hole transport layer (HTL, also known as a back buffer) or as a contact electrode (such as indium tin oxide, ITO) exhibit high transparency for light with photon energies greater than the CdTe bandgap energy.

Bifacial PV device designs are common for crystalline silicon solar cells but thin-film bifacial devices based on, e.g., CdTe, are limited [4,5]. For the development of high efficiency bifacial PV cells, optically transparent p-type materials with band edge energies aligned to CdTe are desired [6]. Tiwari et al. used ITO as a transparent back contact layer to CdTe solar cells and reported front and rear efficiencies of 7.9% and 1.0% respectively [7]. Romeo et al. reported front and rear efficiencies of 8.0% and 3.2%, for a CdTe layer thickness of 1.0 μm, when inserting a thin copper layer between the CdTe and the ITO back electrode [8]. Usually, a thin absorber layer is preferred for collecting photons incident from the back surface, although front-illuminated efficiency drops for CdTe absorber layers below ~1 μm. The back-illumination device efficiency is low compared to front illumination due to inefficient current collection (J_{SC}) since electron-hole pairs are generated far from the

* Corresponding author.
E-mail address: Randy.Ellingson@utoledo.edu (R.J. Ellingson).

https://doi.org/10.1016/j.solmat.2021.111451
Received 17 June 2021; Received in revised form 16 October 2021; Accepted 18 October 2021
Available online 3 November 2021

diode junction and the corresponding charge-separating electric field. An efficient bifacial CdTe device can be fabricated when the recombination losses at the back interface can be minimized by engineering upward band bending, reducing the downward band bending, or through surface defect passivation [9]. Recently, transparent oxide materials such as aluminum oxide (AlO_x), or copper aluminum oxide (Cu_xAlO_y) have shown improved the minority carrier lifetime for CdTe films indicating reduced back interface recombination current densities [10,11]. Subedi et al. demonstrated solution-based Cu_xAlO_y as a back buffer layer to improve the photogenerated carrier lifetime of CdTe films, achieving a back-illuminated conversion efficiency of 7.1% for a CdS/CdTe device (3.3 μm thick absorber) [11]. There are limited p-type wide band gap semiconductor materials and among them, copper iodide (CuI) is also one of the promising hole transport materials for fabrication of solar cells [12].

Copper iodide is a transparent semiconductor in visible region with three crystalline phases namely α-CuI (above 392 °C), β -CuI (between 350 and 392 °C) and γ-CuI (below 350 °C) [13,14]. The γ -CuI has zinc blende crystal structure with p-type conductivity, band gap of ~3.1 eV, low resistivity in the order of 10^{-2} Ω-cm, high mobility of 43.9 $cm^2 V^{-1} s^{-1}$ and high carrier concentration (10^{18} cm^{-3}) [15–18]. Because of its superior electronic properties and relatively deep work function of (~5.4 eV) [19], CuI has been demonstrated as an effective HTL in perovskite [12,20] and dye-sensitized solar cells [21,22]. In addition, thermally evaporated CuI thin films have been tested as a back interfacial layer in CdTe photovoltaics [23]. Due to high transparency, high optical band gap and suitable location of the Fermi energy level, CuI can serve as a good p-type HTL for the fabrication of bifacial CdTe solar cells.

We have investigated the role of solution-processed CuI nanoparticles (NPs) as a HTL for front and back illuminated CdTe solar cells. Cadmium telluride PV devices with a CuI NP HTL show a PCE as high as 14.8% with FF of 79.2% for a CuI/Au back contact design, whereas the control device (using an Au electrode without CuI HTL) shows the best cell efficiency of 14.0%. Further, we demonstrated a bifacial device utilizing CuI NPs with ITO back electrode with PCEs of 11.6% and 5.5% for front and back illumination respectively. For a bifacial device with CuI/ITO back electrode, the J_{SC} obtained is 12.0 $mAcm^{-2}$ under back illumination for a relatively thick absorber layer (~ 3.5 μm). These PCEs on front and back illumination with CuI NPs were significantly enhanced compared to a reference bifacial device without CuI NPs. Based on the temperature-dependent current voltage (J-V-T) characteristics, the CuI interfacial layer reduced the electronic potential barrier which can severely impede transport of holes to the back electrode (Au or ITO). Additionally, capacitance-voltage (C–V) measurements and impedance spectroscopy (IS) analysis showed increased doping density and improved back interface performance for devices with the CuI interfacial layer.

2. Experimental section

2.1. Chemicals

Copper Iodide (CuI, 99.99%), Acetonitrile (99.8%), Dimethylformamide (DMF, 99.8%) from Sigma Aldrich, Cadmium Chloride (99.99%) from Alfa Aesar and Methanol (99.8%) from Fisher Scientific were purchased and used without further purification.

2.2. Synthesis of CuI nanoparticles

To synthesize CuI NPs, a procedure reported previously by Yang et al. was adopted [24]. For a typical synthesis, 95 mg (0.5 mmol) of CuI was dissolved in 5 mL of acetonitrile under ultrasonic stirring to obtain a transparent pale-yellow solution, and 10 mL of DMF was added into it. The solution was allowed to evaporate till the color of the solution turned green. Subsequently, 10 mL of water was slowly added while stirring as the solution gradually changes from clear to cloudy. The ultrafine white particles were separated from the solution after using centrifugal separation at 5000 rpm for 3 min, indicating the formation of CuI NPs which were dispersed in DMF for further characterization.

2.3. Device fabrication

The CdS/CdTe film stacks obtained from Willard and Kelsey Solar Group were fabricated via vapor transport deposition (VTD) onto TEC™-15 M (Pilkington N.A) glass substrates and were used to test CuI NPs as hole transport materials. A wet $CdCl_2$ treatment was carried at 387 °C to activate CdTe devices using a saturated $CdCl_2$ solution in methanol in dry air environment. The CdTe devices were rinsed with methanol twice after the $CdCl_2$ treatment to remove the excess $CdCl_2$ from the CdTe surface. The CdTe device with $CuCl_2$/Au back contact serves as the controlled device, and we followed a procedure reported previously to complete control devices with $CuCl_2$ treatment [25]. To investigate the effect of CuI NPs as an HTL, 5 mg of as synthesized CuI NPs were dispersed in 1 mL of DMF and 40 μL solution was dropped and spin coated onto CdTe films at 500 and 3000 rpm for 10 s and 30 s respectively. The devices were then annealed for different times (no anneal, 5, 10 and 15 min) at 200 °C. Finally, monofacial devices were completed with a 40 nm Au back metal which was thermally evaporated at a base pressure of 3.0×10^{-6} Torr using a tungsten boat. During the Au deposition, a shadow mask was used to define an active cell area of 0.08 cm^2. Similarly, to prepare a bifacial solar cell (Glass/-FTO/CdS/CdTe/CuI/ITO) after deposition of CuI NPs, ~250 nm of ITO was deposited using RF sputtering at 2 mTorr Ar pressure, and 100 W power at room temperature. After deposition of ITO, devices were manually scribed by making cells of an active area of approximately 0.08 cm^2.

2.4. Characterization

The X-ray diffraction patterns, and UV–vis absorbance spectra of CuI NPs were recorded by using Rigaku Ultima III X-ray diffractometer (40 kV accelerating voltage and 44 mA currents) and PerkinElmer Lambda 1050 UV/Vis/NIR spectrometer respectively. The surface morphologies of CuI NPs were examined with Hitachi S-4800 scanning electron microscopy (SEM). The Raman spectra vibrational peaks of CuI NPs were measured by using Confocal Raman Spectrometer using He–Ne laser with line excitation at 632 nm. The current density-voltage (*J-V*) characteristics of the devices were measured using a Keithley 2400 digital source meter under the illumination of 100 mW/cm^2 of AM1.5G irradiance. The external quantum efficiency (EQE) measurements were performed by PV Instruments (model IVQE8-C) system. Temperature-dependent current voltage measurements (J-V-T) were performed using a Keithley 2401 source meter for current-voltage data acquisition. Capacitance-voltage (C–V) and impedance spectroscopy (IS) measurements were performed using a Solarton Modulab Potentiostat equipped with a frequency response analyzer (Ametek, Inc.) The room temperature photoluminescence (PL) measurements were performed with 532 nm and 633 nm cw laser with a beam diameter ~100 μm and ~180 μm at 3.3 W/cm^2 and 450 mW/cm^2 from back and front side respectively. PL signal was detected by a Horiba Symphony-II CCD detector (integration time = 0.5 s) after a 300 g mm^{-1} grating monochromator. The room temperature time-resolved photoluminescence (TRPL) measurements of CdTe samples were carried with a 532 nm and 633 nm pulsed laser with beam diameter ~150 μm at 113 mW/cm^2 (average power = 20 μW) and 34.5 mW/cm^2 (average power = 6.1 μW) with the repetition rate of 20 MHz and 1 MHz from back and front side illumination respectively. The sample signals were detected at the peak emission wavelength, as determined from the steady state PL measurements. Both front and back side TRPL measurements of CdTe samples were performed using time correlated single photon counting (TCSPC) with an integration time of 600 s. Bi-exponential PL decays were observed.

3. Results and discussion

Fig. 1 displays the characteristics of the synthesized CuI NPs including surface morphology, X-ray diffraction pattern and optical properties. The SEM image in Fig. 1(a) shows morphology and nano-structure of CuI NPs. From SEM image, we can see that the shape of individual NPs is spherical though these NPs agglomerate together and form a granular structure. The XRD pattern in Fig. 1(b) reveals the formation of γ-CuI with lattice constants $a = b = c = 0.60516$ nm in zinc blende structure matching the diffraction patterns with PDF # 97-016-3427 (MDI JADE). The crystallite size of the CuI NPs was estimated from the diffractogram, using the Debye-Scherrer equation given by $D_p = \frac{K\lambda}{\beta cos\theta}$ where D_p is the crystallite size, ($K = 0.9$) is the shape factor, ($\lambda = 0.15406$ nm) is the wavelength of the x-ray, β is the full width at half maximum (FWHM) and θ is the Bragg's diffraction angle [26]. The crystallite size was estimated based on the diffraction peaks at (111), (220), and (311) using OriginPro software. The average crystallite size of CuI NPs is ~37 ± 6 nm. Fig. 1(c) shows the UV–vis absorption spectrum of CuI NPs in solution prepared in DMF recorded in a cuvette of 1 mm pathlength with solvent correction. Based on the absorption spectrum, the energy band gap was estimated to be 3.0 eV, in agreement with results reported previously [23,27,28]. Fig. 1(d) shows the Raman spectrum of CuI NPs obtained using 632.8 nm He–Ne laser source. The transverse optic (TO) vibration mode of CuI NPs is obtained at 122.5 cm^{-1} which agrees closely with a previous report [28].

CuI thin films have carrier concentration in the order of 10^{18} cm^{-3} having a valence band at −5.4 eV with respect to vacuum [18,19]. The valence band edge of CuI is very close to that of CdTe suggesting its suitability for hole extraction at the CdTe back contact. Fig. 2(a) shows the non-interacting band diagram of CdS/CdTe solar cells with CuI as an HTL. Based on the literature, there exists a very small valence band offset (~0.08 eV) between CdTe and CuI thin film prepared by thermal evaporation method [23]. Fig. 2(b) and (c) show the SEM images of $CdCl_2$ treated CdTe devices without and with CuI NPs on top of CdTe surface respectively. The SEM image in Fig. 2(c) shows the features different from bare CdTe surface due to these CuI NPs.

Fig. 3 displays the statistical distribution of device parameters of CdS/CdTe solar cells with and without CuI NPs. In our laboratory, $CuCl_2$/Au is often used as a control back contact. Here, we have completed CdTe devices with various contacts: Au only, $CuCl_2$/Au, and CuI/Au. The devices dipped in $CuCl_2$ were annealed at 200 °C for 20 min [25] while devices with CuI NPs (omitting $CuCl_2$) were annealed at 200 °C for 0, 5, 10 and 15 min. The *J-V* curves, their corresponding EQEs, and device parameters of the best cells of each back contact type are presented in Fig. S1 and Table S1. The control device using $CuCl_2$/Au shows PCE of 14.0% similar to our previous results [30,31], whereas the device with CuI NPs (unannealed) shows a similar PCE of 14.1%. Further, we studied the effect of heat treatment on these devices after the deposition of the CuI NPs layer. Without any post-CuI annealing, the FF of the best device was 76.0%, whereas after annealing for 5 min at 200 °C, FF increased to 79.2%. On further annealing, FF starts to decrease (77.5% for 10 min, and 75.9% for 15 min). As we see from Fig. 3(a), there is no significant difference in V_{OC} of the device annealed for 5 min as compared to room temperature. However, V_{OC} increases up to 10 min annealing, and decreases again for 15 min. The increase in V_{OC} and FF after annealing is attributed to diffusion of copper from the CuI NPs into the CdTe. The highest PCE observed was 14.8% for 5 min annealing time. The device performance of nearly 15.0% is quite impressive for CdTe devices which include the CdS window layer since parasitic optical absorption in the CdS yields a lower J_{SC} (~22.0 $mAcm^{-2}$) as compared to other window layers (~29.0 $mAcm^{-2}$) such as CdS:O, CdSe or magnesium zinc oxide (MZO) [32,33]. We also used steady state PL and TRPL measurements (Fig. S2) to analyze the CdTe

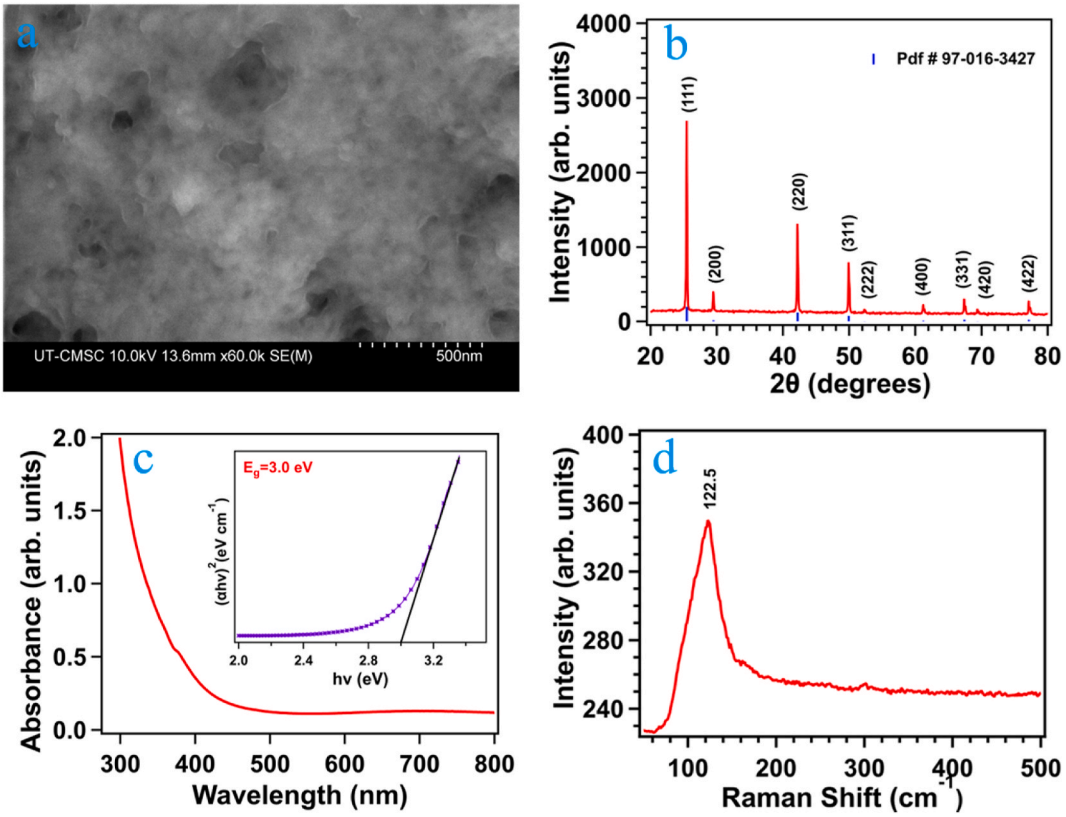

Fig. 1. (a) SEM image of CuI NPs (b) XRD pattern of CuI NPs on soda lime glass, the vertical blue color lines correspond to PDF # 97-016-3427 (MDI JADE) (c) UV–vis absorption spectrum of CuI NPs solution prepared in DMF; the inset shows the optical band gap, (d) Raman spectroscopy measurement of CuI NPs using 632.8 nm excitation of He–Ne laser. (For interpretation of the references to color in this figure legend, the reader is referred to the Web version of this article.)

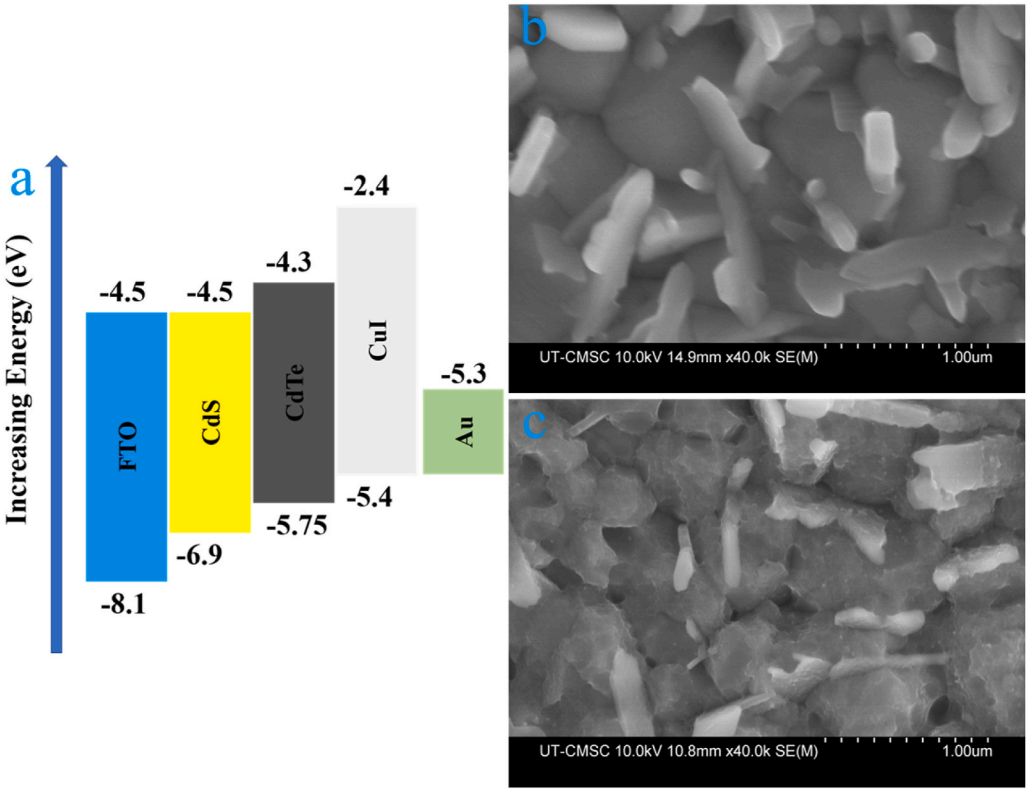

Fig. 2. (a) Non-interacting band diagram for a typical CdTe device with structure FTO/CdS/CdTe/CuI/Au showing the position of valence band and conduction band edges with respect to the vacuum level [5,29]. SEM images of CdTe devices (b) without and (c) with CuI NPs on CdTe surface.

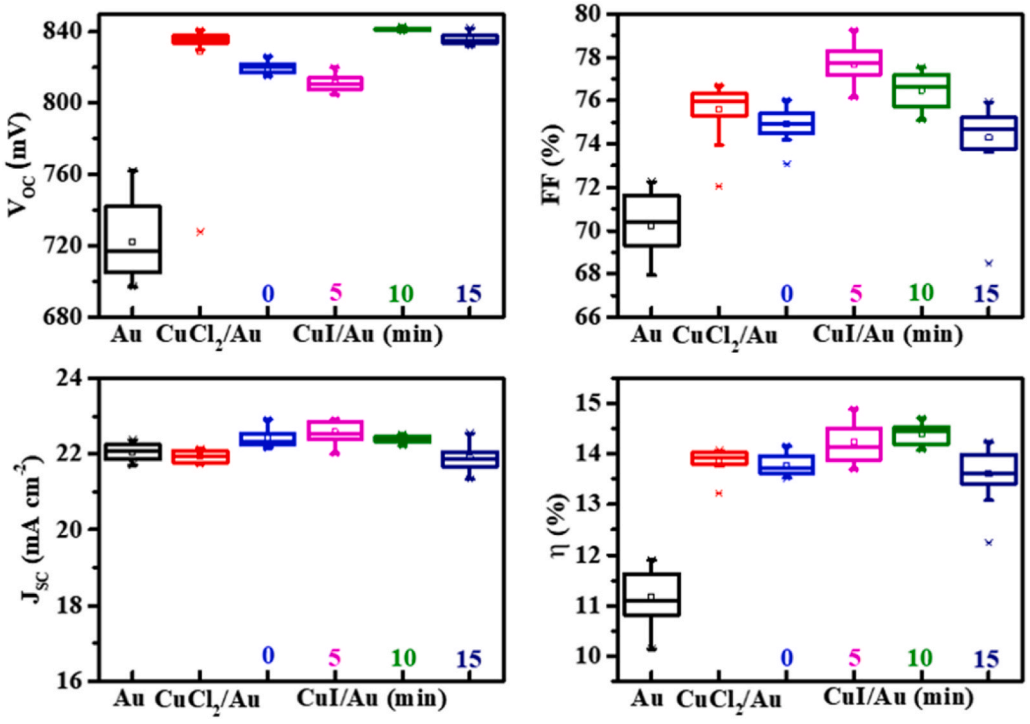

Fig. 3. Statistical distribution of solar cells parameters (V_{OC}, J_{SC}, FF, and η) from 15 cells of the CdTe devices with Au only, $CuCl_2$/Au (controlled device) and CuI/Au back contacts respectively. The CuI/Au back contacts were annealed at 200 °C for 0, 5, 10 and 15 min respectively.

devices with and without CuI NPs at the back. With the introduction of the CuI as the HTL, the PL intensity from both front and back side illumination were decreased. When compared with the control device which omits the CuI NP film, the minority carrier lifetime decreases from 12.5 ns to 8.0 ns for front illumination, and from 0.8 ns to 0.6 ns for back illumination. The decrease in PL and minority carrier lifetime is consistent with the idea that CuI assists with efficient charge carrier separation in its function as an HTL.

Furthermore, as CuI is a transparent semiconductor, we extended our work to a bifacial configuration with ITO as a transparent back electrode and analyzed device performances. Fig. S3 shows the non-interacting band diagram of bifacial CdS/CdTe solar cells with a device structure Glass/FTO/CdS/CdTe/CuI/ITO. We compared our results to ITO back electrode directly on CdTe (with no Cu doping step), and to $CuCl_2$/ITO. Fig. 4(a and b) shows *J-V* characteristics and EQEs of the best cell of ITO only, $CuCl_2$/ITO and CuI/ITO devices with front and back illumination. The solid lines correspond to back illumination and dotted lines correspond to front illumination respectively. The ITO-only device has PCE of 1.1% with J_{SC} of 5.5 $mAcm^{-2}$ for back illumination while for $CuCl_2$/ITO device efficiency is 3.0% with J_{SC} of 7.9 $mAcm^{-2}$. The V_{OC} was significantly improved for $CuCl_2$ treated devices with ITO back contact for both front and back illuminations. With implementing CuI NPs in between CdTe layer and ITO electrode, PCE of 5.5% was observed with J_{SC} 12.0 $mAcm^{-2}$ for back illumination and 11.6% for front illumination. The device parameters for the best cells of ITO, $CuCl_2$/ITO, and CuI/ITO back contacts with front and back illuminations are presented in Table 1.

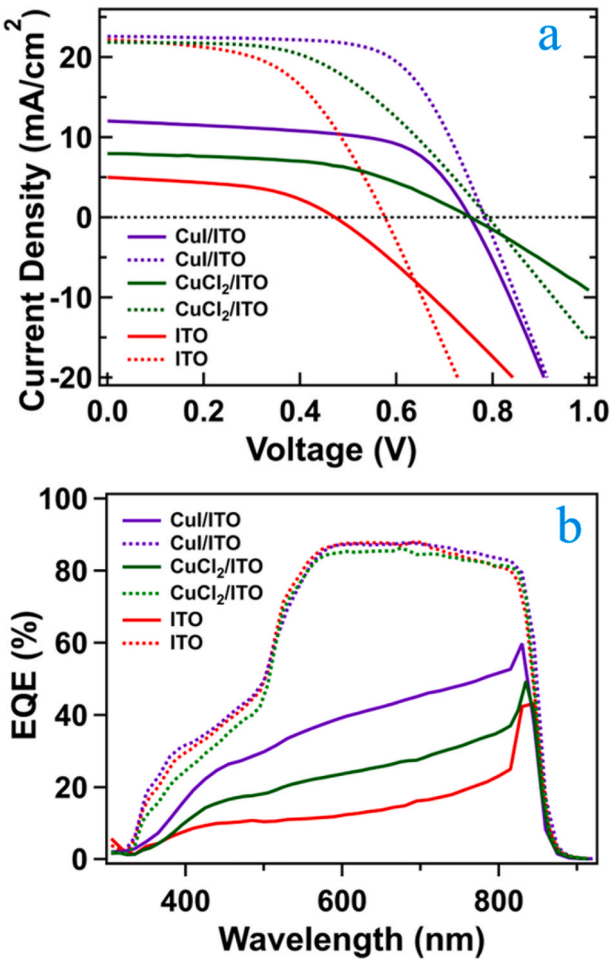

Fig. 4. Performance of bifacial CdTe solar cells with ITO and $CuCl_2$/ITO, CuI/ITO back electrode illuminated from back and front (a) *J-V* characteristics and (b) EQEs. Solid and dotted lines correspond to back and front side illuminations respectively under AM1.5 solar spectrum.

There is a significant improvement in J_{SC} and FF with CuI NPs for bifacial CdTe solar cells as compared to ITO and $CuCl_2$/ITO back contacts. However, the FF is lower with ITO back electrode as compared to opaque configuration (with Au) as ITO has a high sheet resistance of ~34 Ω/sq. Similarly, the statistical distributions of V_{OC}, J_{SC}, FF and η of all back contacts for back and front illuminations are presented in Figs. S4 and S5. The use of CuI NPs as an HTL layer between CdTe and ITO back electrode shows significant increase in device performance due to the increase in J_{SC} and FF for back illumination. We attribute this increase to improved band alignment of CdTe with CuI, and reduced downward band bending at the back electrode when using the CuI NP HTL.

The sum of front- and back-illuminated efficiencies for ITO-only back contact is 8.1% which is comparable to previously reported results [34]. Subedi et al. reported a bifacial CdTe device with front and back illumination efficiencies of 13.3% and 1.2% respectively using barium copper sulfide as the back interface layer to 3.5 μm thick CdTe solar cells [35]. Marsillac et al. reported front- and back-illuminated efficiencies of 5.7% and 5.0% respectively with ZnTe:N buffer layer to ultra-thin bifacial CdTe solar cells for 0.68 μm [36]. Subedi et al. have reported the bifacial device with efficiency 5.5% with J_{SC} 10.8 $mAcm^{-2}$ using Cu_xAlO_y buffer layer, and it was further enhanced to 7.1% with J_{SC} 12.9 $mAcm^{-2}$ with MgF_2 coating for 3.3 μm CdTe when illuminated from the back [11]. For CuI buffer layer, the J_{SC} value obtained is 12.0 mA cm^{-2} when illuminated from the back, without any antireflection coating. Compared to other transparent or semi-transparent HTLs, CuI NPs showed comparable or improved device performance for bifacial CdS/CdTe devices, especially for the back-illuminated performance, owing the highly transparent property of CuI in the visible region [37]. The peak in carrier collection observed near 800 nm in the EQE curve is due to the carrier collection near the CdS/CdTe junction. Since photogenerated electrons originating near the back-contact must reach the front electrode, there is a high probability of recombination loss and current density is reduced for back illumination, and especially for shorter wavelengths of light which predominantly absorbed nearer to the back contact [7,38]. For improved performance of the devices from back side illumination, reduced downward band bending or the chemical/field effect passivation of the back interface is essential [9]. Here, CuI may reduce the downward band bending on the back interface, lowering the back barrier height while helping to reduce the recombination at the back interface. As a result, the J_{SC} and FF were greatly improved for CuI/ITO compared to $CuCl_2$/ITO and ITO-only back contact. We further studied the effect of these back contacts using temperature dependent current-voltage measurement (J-V-T), capacitance voltage (C–V) and impedance spectroscopy (IS).

To study and analyze the potential barrier at the back-contact interface, J-V-T measurements were performed under dark conditions varying temperature from 190 to 300 K. To calculate the back-barrier height (φ_b), we assume the thermionic emission model given by an equation,

$$J_o \propto T^2 . exp[\frac{-q.\varphi_b}{k_B T}] \quad (1)$$

Where J_0 is the saturation current, q is an electronic charge, k_B is the Boltzmann constant and T is the temperature [39]. Fig. 5(a) shows the plots of ln (J_0/T^2) versus $1/k_BT$ for CdTe solar cells with $CuCl_2$/Au, CuI/Au, $CuCl_2$/ITO, and CuI/ITO back contacts to extract the back-barrier height of the devices. Based on the analysis and fitting as shown in Fig. S6 and Fig. 5(b), the back-barrier height for $CuCl_2$/Au, CuI/Au, $CuCl_2$/ITO, and CuI/ITO are 315 ± 7 meV, 224 ± 2 meV, 331 ± 4 meV and 187 ± 4 meV respectively. By introducing CuI NPs as an HTL, the back-barrier height was reduced for both Au and ITO back electrode indicating the decrease in contact resistance and better transport of holes towards the back electrode. Additionally, the decrease in back-barrier height is attributed to the increase in V_{OC} and FF of the devices as discussed in (Table 1 and Table S1). The reduction in barrier

Table 1
The device performance parameters (V_{OC}, J_{SC}, FF, η, R_S, R_{SH}) of the best cells for ITO, $CuCl_2$/ITO, and CuI/ITO devices with front and back illumination.

Back Contacts	Illumination	V_{OC} (mV)	J_{SC} ($mAcm^{-2}$)	FF (%)	η (%)	R_S ($\Omega\ cm^2$)	R_{SH} ($\Omega\ cm^2$)
ITO	Front	576	22.3	52.1	7.0	8.8	539
	Back	473	5.0	48.5	1.1	24.0	330
$CuCl_2$/ITO	Front	790	21.8	50.1	8.6	13.6	3878
	Back	754	7.9	51.4	3.0	28.6	747
CuI/ITO	Front	784	22.5	66.1	11.6	5.7	4604
	Back	753	12.0	60.8	5.5	8.1	400

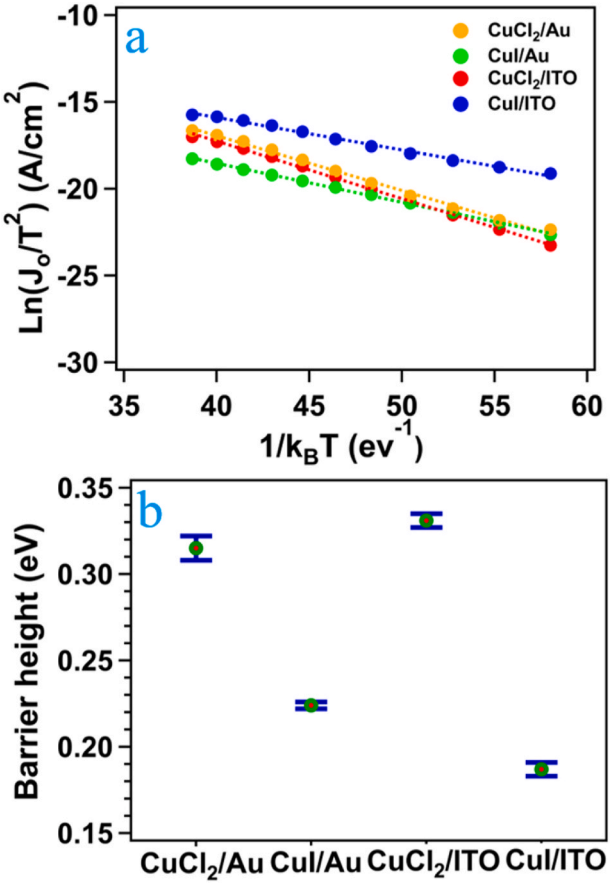

Fig. 5. a) J-V-T characteristics of $CuCl_2$/Au, CuI/Au, $CuCl_2$/ITO, and CuI/ITO back contact devices, plots of ln (J_0/T^2) versus $1/k_BT$ to calculate back-barrier height of CdTe solar cells and (b) values of back barrier height for $CuCl_2$/Au, CuI/Au, $CuCl_2$/ITO, and CuI/ITO back contacts.

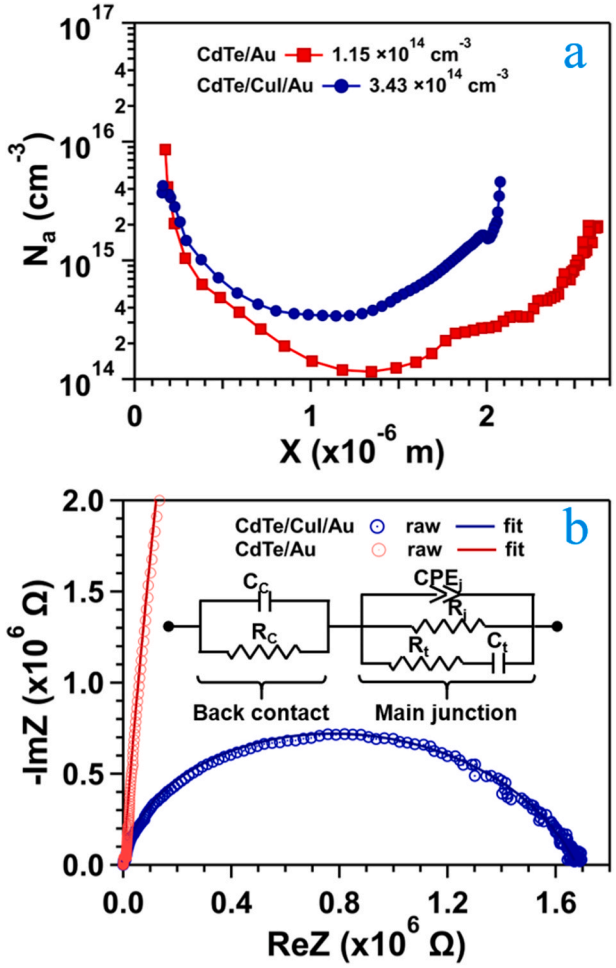

Fig. 6. (a) capacitance-voltage (C–V) measurements to determine carrier density of CdTe devices without CuI and with CuI NPs. (b) Raw and fit complex impedance spectra (Nyquist plots) of CdS/CdTe solar cell devices without and with CuI treatment. The inset is the equivalent circuit model that is used for the fitting, where with the elements R, C, and CPE represent the resistance, capacitance, and constant phase element, respectively, with two sub-circuits connected in series, one is due to the back-contact (subscript c) and the other part due to the p-n junction and the bulk material (subscripts j and t, respectively).

height with CuI NPs should be accompanied with similar reduction in band bending, which in turn reduces recombination at the back and enhances device performance.

To investigate the carrier concentration in CdTe devices, the room temperature C–V measurements were performed in the dark with a constant AC voltage of 45 mV_{rms} and frequency of 10 kHz. AC signals were superimposed on a DC bias voltage varying from −2.5 to +0.8 V. Fig. 6 (a) shows the carrier concentration profiling vs. depth in CdTe solar cells with and without CuI NPs. The carrier density of the device with CuI (CdTe/CuI/Au) is 3.43×10^{14} cm^{-3} that is slightly higher than the device without CuI (1.15×10^{14} cm^{-3}). The result suggests that the modest increase in carrier density may be due to copper diffusion during post annealing treatment that was performed at 200 °C for 10 min. We employed IS to study the impact of CuI treatment on the properties of the back-contact and the main junction CdTe solar cell devices. The IS measurements were done with frequency sweeping from 1.0 MHz to 0.01 Hz under dark equilibrium and a constant AC modulation voltage

Table 2
Summary of the fit circuit elements (back-contact) from the impedance spectra CdS/CdTe solar cell devices without and with CuI treatment.

Device	R_C (Ω)	C_C (F)	R_j (Ω)	σ ($\Omega^{-1}\ cm^{-1}$)
With CuI	3.75×10^3	9.28×10^{-10}	7.10×10^5	6.16×10^{-9}
Without CuI	9.69×10^5	2.32×10^{-9}	1.49×10^9	2.93×10^{-12}

of 45 mV_{rms}. First, we used the equivalent circuit model reported by Awni et al. [40] to fit the complex impedance spectra, as shown in Fig. 6 (b).

The fit circuit elements from the impedance spectra of CdS/CdTe solar cell devices without and with CuI treatment are summarized in Table 2. We found that the fitted back-contact (R_C) for CuI treated device ($3.75 \times 10^3\ \Omega$) is lower than the control device ($9.69 \times 10^5\ \Omega$) by ~ two orders and the fitted back contact capacitance (C_C) of CuI treated device is lower (9.28×10^{-10} F) than that of the control device (2.32×10^{-9} F). The decrease of the back-contact resistance and capacitance indicates that the holes are more freely to move and transfer with less accumulation near the CdTe/metal interface which could be due to reducing electron flow from the absorber layer to the back surface in the device with CuI layer. However, without CuI layer, the high back-contact resistance plays the major role in the charge transport mechanism. The back-contact resistance results in non-ohmic back-contact and creates a barrier. This barrier creates undesired downward band bending near the CdTe/metal interface which fails to repel electrons toward the front contact's p-n junction, and instead promotes recombination near the back contact. The bulk conductivity (σ) has been calculated using the fitted junction resistance (R_j) by using the relation $\sigma = \frac{t}{AR_j}$, where t and A are the absorber thickness and active area. We found that the conductivity of CdS/CdTe devices with CuI layer ($6.16 \times 10^{-09}\ \Omega^{-1}\ cm^{-1}$) is higher than the control device ($2.93 \times 10^{-12}\ \Omega^{-1}\ cm^{-1}$), which may be due to Cu diffusion.

4. Conclusions

Here, we synthesized CuI NPs utilizing solution processing and investigated its role as an HTL in CdTe devices for opaque and transparent back contacts. When CuI NPs were used with proper annealing, the device performance was improved compared to $CuCl_2$ treated devices mainly due to the improvement in FF which is attributed to the reduced back barrier height of the device. CdTe devices with CuI/ITO back contact produced promising results as bifacial devices with 11.6% and 5.5% device efficiency from front and back illumination respectively. The significant enhancement in current collection (12.0 $mAcm^{-2}$) was observed when using CuI as a back-buffer layer, with ITO as the transparent back electrode, when the device was illuminated from the back. The improvement in device parameters is due to lower back-barrier height and is consistent with reduced downward band bending at the back electrode of the device. The development of bifacial devices using these CuI NPs is a significant step forward to realize bifacial thin film PV technology.

CRediT authorship contribution statement

Dipendra Pokhrel: Conceptualization, Investigation, Formal analysis, Writing – original draft. **Ebin Bastola:** Formal analysis, Experimental and analytical support, Writing – review & editing. **Kamala Khanal Subedi:** Investigation, Formal analysis, PL and TRPL measurements and analysis. **Suman Rijal:** Investigation. **Manoj K. Jamarkattel:** Investigation, Formal analysis, JVT measurements and analysis. **Rasha A. Awni:** Investigation, Formal analysis, CV and Impedance Spectroscopy measurements and analysis. **Adam B. Phillips:** Supervision. **Yanfa Yan:** Supervision, Funding acquisition. **Michael J. Heben:** Supervision, Funding acquisition. **Randy J. Ellingson:** Project administration, Supervision, Writing – review & editing, Funding acquisition.

Declaration of competing interest

The authors declare that they have no known competing financial interests or personal relationships that could have appeared to influence the work reported in this paper.

Acknowledgment

This material is based on research sponsored by Air Force Research Laboratory under agreement number FA9453-18-2-0037, FA9453-19-C-1002, and by the U. S. DOE's office of Energy Efficiency and Renewable Energy (EERE) under Solar Energy Technologies Office (SETO) Agreement DE-EE0008974. The U.S. Government is authorized to reproduce and distribute reprints for Governmental purposes notwithstanding any copyright notation thereon. The views and conclusions contained herein are those of the authors and should not be interpreted as necessarily representing the official policies or endorsements, either expressed or implied, of Air Force Research Laboratory or the U.S. Government. We also thank Willard and Kelsey Solar Group for providing CdS/CdTe device stacks.

Appendix A. Supplementary data

Supplementary data to this article can be found online at https://doi.org/10.1016/j.solmat.2021.111451.

References

[1] D. Bonnet, P. Meyers, Cadmium-telluride—material for thin film solar cells", J. Mater. Res. 13 (10) (1998) 2740.
[2] B.E. McCandless, J.R. Sites, Cadmium telluride solar cells, Handbk Photovolt. Sci. Eng. 600 (2011).
[3] J.N. Duenow, W.K. Metzger, Back-surface recombination, electron reflectors, and paths to 28% efficiency for thin-film photovoltaics: a CdTe case study, J. Appl. Phys. 125 (5) (2019), 053101.
[4] J. Pang, Y. Cai, Q. He, H. Wang, W. Jiang, J. He, T. Yu, W. Liu, Y. Zhang, Y. Sun, Preparation and characteristics of MoSe2 interlayer in bifacial Cu (In, Ga) Se2 solar cells, Phys. Procedia 32 (2012) 372.
[5] K.K. Subedi, E. Bastola, I. Subedi, Z. Song, K.P. Bhandari, A.B. Phillips, N. J. Podraza, M.J. Heben, R.J. Ellingson, Nanocomposite $(CuS)_x$ $(ZnS)_{1-x}$ thin film back contact for CdTe solar cells: toward a bifacial device, Sol. Energy Mater. Sol. Cell. 186 (2018) 227.
[6] X. Xu, J. Bullock, L.T. Schelhas, E.Z. Stutz, J.J. Fonseca, M. Hettick, V.L. Pool, K. F. Tai, M.F. Toney, X. Fang, Chemical bath deposition of p-type transparent, highly conducting $(CuS)_x$:$(ZnS)_{1-x}$ nanocomposite thin films and fabrication of Si heterojunction solar cells, Nano Lett. 16 (3) (2016) 1925.
[7] A.N. Tiwari, G. Khrypunov, F. Kurdzesau, D. Bätzner, A. Romeo, H. Zogg, CdTe solar cell in a novel configuration, Prog. Photovoltaics Res. Appl. 12 (1) (2004) 33.
[8] A. Romeo, G. Khrypunov, S. Galassini, H. Zogg, A. Tiwari, Bifacial configurations for CdTe solar cells, Sol. Energy Mater. Solar Cells 91 (15–16) (2007) 1388.
[9] A.B. Phillips, K.K. Subedi, G.K. Liyanage, F.K. Alfadhili, R.J. Ellingson, M.J. Heben, Understanding and advancing bifacial thin film solar cells", ACS Appl. Energy Mater. 3 (7) (2020) 6072.
[10] C.L. Perkins, T. Ablekim, T.M. Barnes, D. Kuciauskas, K.G. Lynn, W. Nemeth, M. O. Reese, S.K. Swain, W.K. Metzger, Interfaces between CdTe and ALD Al_2O_3, IEEE J. Photovolt. 8 (6) (2018) 1858.
[11] K.K. Subedi, A.B. Phillips, N. Shrestha, F.K. Alfadhili, A. Osella, I. Subedi, R. A. Awni, E. Bastola, Z. Song, D.-B. Li, Enabling bifacial thin film devices by developing a back surface field using CuxAlOy, Nano Energy (2021) 105827.
[12] W. Sun, S. Ye, H. Rao, Y. Li, Z. Liu, L. Xiao, Z. Chen, Z. Bian, C. Huang, Room-temperature and solution-processed copper iodide as the hole transport layer for inverted planar perovskite solar cells, Nanoscale 8 (35) (2016) 15954.
[13] W. Bührer, W. Hälg, Crystal structure of high-temperature cuprous iodide and cuprous bromide, in: Presented at the International Symposium on Solid Ionic and Ionic-Electronic Conductors, 1977.
[14] M. Grundmann, F.L. Schein, M. Lorenz, T. Böntgen, J. Lenzner, H. von Wenckstern, Cuprous iodide–ap-type transparent semiconductor: history and novel applications, Phys. Status Solidi 210 (9) (2013) 1671.
[15] H. Wang, X. Bai, J. Wei, P. Li, Y. Jia, H. Zhu, K. Wang, D. Wu, Preparation of CuI particles and their applications in carbon nanotube-Si heterojunction solar cells, Mater. Lett. 79 (2012) 106.
[16] T. Tanaka, K. Kawabata, M. Hirose, Transparent, conductive CuI films prepared by rf-dc coupled magnetron sputtering, Thin Solid Films 281 (1996) 179.
[17] D. Chen, Y. Wang, Z. Lin, J. Huang, X. Chen, D. Pan, F. Huang, Growth strategy and physical properties of the high mobility p-type CuI crystal, Cryst. Growth Des. 10 (5) (2010) 2057.
[18] M. Wang, H. Wei, Y. Wu, C. Yang, P. Han, F. Juan, Y. Chen, F. Xu, B. Cao, Highly transparent and conductive γ-CuI films grown by simply dipping copper films into iodine solution, Phys. B Condens. Matter 573 (2019) 45.
[19] S. Shao, J. Liu, J. Zhang, B. Zhang, Z. Xie, Y. Geng, L. Wang, Interface-induced crystalline ordering and favorable morphology for efficient annealing-free poly (3-hexylthiophene): fullerene derivative solar cells", ACS Appl. Mater. Interfaces 4 (10) (2012) 5704.

[20] H. Wang, Z. Yu, X. Jiang, J. Li, B. Cai, X. Yang, L. Sun, Efficient and stable inverted planar perovskite solar cells employing CuI as hole-transporting layer prepared by solid–gas transformation, Energy Technol. 5 (10) (2017) 1836.
[21] S.A. Mohamed, J. Gasiorowski, K. Hingerl, D.R. Zahn, M.C. Scharber, S.S. Obayya, M.K. El-Mansy, N.S. Sariciftci, D.A. Egbe, P. Stadler, CuI as versatile hole-selective contact for organic solar cell based on anthracene-containing PPE–PPV, Sol. Energy Mater. Sol. Cell. 143 (2015) 369.
[22] S. Das, J.-Y. Choi, T. Alford, P3HT: PC61BM based solar cells employing solution processed copper iodide as the hole transport layer, Sol. Energy Mater. Sol. Cell. 133 (2015) 255.
[23] X. Li, D. Xiao, L. Wu, D. Wang, G. Wang, D. Wang, CdTe thin film solar cells with copper iodide as a back contact buffer layer, Sol. Energy 185 (2019) 324.
[24] Y. Yang, S. Liu, K. Kimura, Synthesis of well-dispersed CuI nanoparticles from an available solution precursor, Chem. Lett. 34 (8) (2005) 1158.
[25] E. Bastola, A.V. Bordovalos, E. LeBlanc, N. Shrestha, M.O. Reese, R.J. Ellingson, Doping of CdTe using $CuCl_2$ solution for highly efficient photovoltaic devices, in: 2019 IEEE 46th Photovoltaic Specialists Conference, PVSC), 2019, p. 1846.
[26] J.I. Langford, A. Wilson, Scherrer after sixty years: a survey and some new results in the determination of crystallite size, J. Appl. Crystallogr. 11 (2) (1978) 102.
[27] M. Xia, M. Gu, X. Liu, B. Liu, S. Huang, C. Ni, Luminescence characteristics of CuI film by iodine annealing, J. Mater. Sci. Mater. Electron. 26 (7) (2015) 5092.
[28] D.K. Kaushik, M. Selvaraj, S. Ramu, A. Subrahmanyam, Thermal evaporated copper iodide (CuI) thin films: a note on the disorder evaluated through the temperature dependent electrical properties, Sol. Energy Mater. Sol. Cell. 165 (2017) 52.
[29] D. Saranin, P. Gostischev, D. Tatarinov, I. Ermanova, V. Mazov, D. Muratov, A. Tameev, D. Kuznetsov, S. Didenko, A. Di Carlo, Copper iodide interlayer for improved charge extraction and stability of inverted perovskite solar cells, Materials 12 (9) (2019) 1406.
[30] D. Pokhrel, E. Bastola, A.B. Phillips, M.J. Heben, R.J. Ellingson, Aspect ratio controlled synthesis of tellurium nanowires for photovoltaic applications, Mater. Adv. 1 (8) (2020) 2721.
[31] D. Pokhrel, E. Bastola, K.K. Subedi, A. Phillips, M.J. Heben, R.J. Ellingson, Solution-processed copper telluride nanowire thin film as a back-buffer layer to cadmium telluride solar cells, in: 2020 47th IEEE Photovoltaic Specialists Conference, PVSC, 2020, pp. 2561–2563.
[32] D.E. Swanson, J.R. Sites, W.S. Sampath, Co-sublimation of CdSexTe1 − x layers for CdTe solar cells, Sol. Energy Mater. Sol. Cell. 159 (2017) 389.
[33] E. Bastola, A.B. Phillips, G. Barros-King, M.K. Jamarkattel, D.B. Li, A. Quader, D. Pokhrel, J.M. Gibbs, Y. Yan, R.J. Ellingson, M.J. Heben, Understanding the interplay between CdSe thickness and Cu doping temperature in CdSe/CdTe devices, IEEE J. Photovolt (2021) 1–5. https://doi.org/10.1109/JPHOTOV.2021.3110338.
[34] E. Byun, J. Seo, D. Kim, J. Kim, Bifacial CdS/CdTe thin-film solar cells with copper nanowires as a transparent back contact, Opt Express 26 (18) (2018) 23594.
[35] K.K. Subedi, E. Bastola, I. Subedi, S.S. Bista, S. Rijal, M.K. Jamarkattel, R.A. Awni, A.B. Philips, Y. Yan, M.J. Heben, Semi-transparent p-type barium copper sulfide as a back contact interface layer for cadmium telluride solar cells, Sol. Energy Mater. Sol. Cell. 218 (2020) 110764.
[36] S. Marsillac, V. Parikh, A. Compaan, Ultra-thin bifacial CdTe solar cell, Sol. Energy Mater. Solar Cells 91 (15–16) (2007) 1398.
[37] P. Storm, M. Bar, G. Benndorf, S. Selle, C. Yang, H. von Wenckstern, M. Grundmann, M. Lorenz, High mobility, highly transparent, smooth, p-type CuI thin films grown by pulsed laser deposition, Apl. Mater. 8 (9) (2020), 091115.
[38] Y. Kwon, J. Seo, Y. Kang, D. Kim, J. Kim, Bifacial CdS/CdTe thin-film solar cells using a transparent silver nanowire/indium tin oxide back contact, Opt Express 26 (2) (2018) A30.
[39] A. Niemegeers, M. Burgelman, Effects of the Au/CdTe back contact on IV and CV characteristics of Au/CdTe/CdS/TCO solar cells", J. Appl. Phys. 81 (6) (1997) 2881.
[40] R.A. Awni, D.-B. Li, Z. Song, S.S. Bista, M.A. Razooqi, C.R. Grice, L. Chen, G. K. Liyanage, C. Li, A.B. Phillips, M.J. Heben, R.J. Ellingson, J.V. Li, Y. Yan, Influences of buffer material and fabrication atmosphere on the electrical properties of CdTe solar cells, Prog. Photovoltaics Res. Appl. 27 (11) (2019) 1115.